Grazing incidence small-angle x-ray scattering study of self-organized SiGe wires

V. Holý,* T. Roch, J. Stangl, A. Daniel, and G. Bauer[†]

Institut für Halbleiterphysik, Johannes Kepler Universität, A-4040 Linz, Austria

T. H. Metzger

European Synchrotron Radiation Facility, F-38042 Grenoble Cedex 9, France

Y. H. Zhu, K. Brunner, and G. Abstreiter

Walter-Schottky Institut, Technische Universität München, D-85748, Germany

The structure of self-organized quantum wires buried at the interfaces of a SiGe/Si multilayer is investigated by grazing incidence small-angle x-ray scattering. A nearly periodic distribution of wires, well described by a short-range ordering model, gives rise to intensity satellite maxima in reciprocal space. The shape of the wire cross section is determined from the heights of these intensity maxima, and the analysis reveals that the conventional step-bunching model is not sufficient to explain the wire shape.

I. INTRODUCTION

The structural characterization of self-organized semiconductor nanostructures has been the subject of intense investigations. In order to understand the electronic and optical properties of such nanostructures, information on their size, shape, composition, and composition gradients, as well as of their strain status is indispensable. So far, most of such studies were focused on quantum *dots* grown in the Stranski-Krastanow growth mode,[1–3] whereas much less work has been devoted to the investigation of self-organized grown quantum *wires*.[4–6] It has been shown that the growth of such wires requires a suitable template, which can be provided, e.g., by regular arrays of terraces formed during a step-bunching growth process.[7–9] Such step-bunching instabilities have been observed to occur in several systems, including Si/SiGe multilayers grown on miscut Si substrates. Brunner *et al.*[10] have shown recently that for molecular-beam epitaxy (MBE) growth of SiGe nanostructures, certain ranges of growth parameters exist, where either laterally ordered SiGe island growth takes place, or wires are formed on nearly equally spaced terraces, which were studied by transmission electron microscopy and atomic force microscopy (AFM).

For the nondestructive characterization of *etched*, *free-standing* periodic wires, x-ray diffraction and scattering techniques have been frequently used (see, e.g., Ref. 11), in particular to study their shape and strain status. However, the observation of optical properties like luminescence requires that the wires are embedded into a matrix, i.e., they have to be overgrown, which is usually accompanied by a dramatic change of their shape, size, and composition.[12,13] It is the purpose of this paper to investigate in particular the *shape and size* of *buried* self-organized SiGe wires, using grazing incidence small-angle x-ray scattering techniques.

II. EXPERIMENT

We have studied a 20 period SiGe/Si multilayer, which was grown by solid source MBE on a [001]-oriented Si sub- strate with a miscut of 3.5° towards the [100] direction. With the chosen growth conditions, a smooth Si buffer was grown.[14] The thickness of the $Si_{0.55}Ge_{0.45}$ and Si layers was nominally 2.5 nm and 10 nm, respectively. The whole multilayer stack was covered by a 12-nm-thick Si capping layer. The substrate temperature during multilayer growth was 550 °C; for growth details see Ref. 10. The surface morphology of the top Si layer was investigated by AFM and is shown in Fig. 1, together with its two-dimensional Fourier transform. We observe a one-dimensional periodic ripple structure along the miscut direction [100], with a lateral period of about 90 nm. Additionally, some ''holes'' in the surface are observed, with typical distances much larger than the period of the ripples, and random distribution.

X-ray diffraction from self-organized quantum wires is mainly influenced by the *strain fields* in the Si matrix caused by the buried SiGe wires. In order to get a direct information
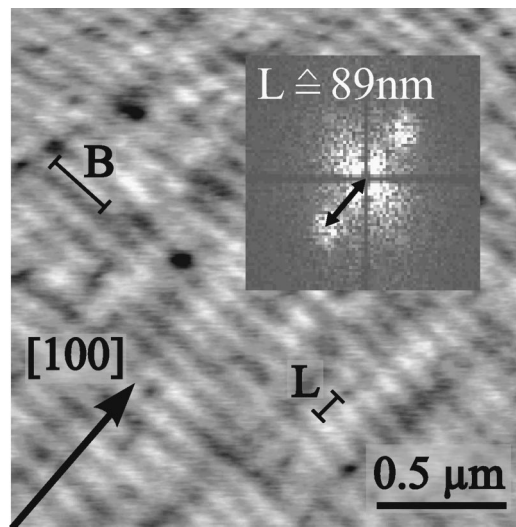
FIG. 1. Surface morphology obtained by AFM, the inset shows the two-dimensional Fourier transform. The arrow indicates the miscut direction. *B* indicates the average wire length.
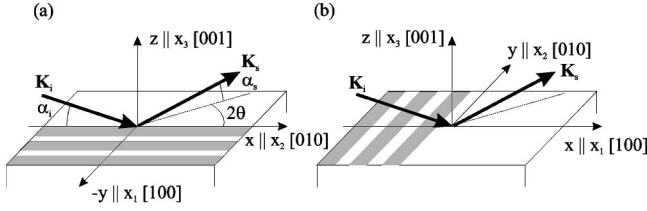
FIG. 2. Sketch of the GISAXS scattering geometry for the incidence plane parallel (a) and perpendicular (b) to the wire direction of the wires (gray stripes).

on the wire *shape*, here strain-insensitive small-angle x-ray scattering has been applied. We used the grazing-incidence small-angle x-ray scattering geometry (GISAXS), where the scattering plane is nearly parallel to the sample surface (Fig. 2), and a large range of in-plane momentum transfer can be investigated. The experiments were carried out at the undulator beamline TROIKA II at the ESRF, Grenoble, using a wavelength of $\lambda = 0.155$ nm. The diffusely scattered intensity from the buried nanostructures was measured by a position sensitive detector oriented parallel to the sample surface, i.e., parallel to the Q_y axis. During a GISAXS scan the angles $\alpha_{i,s}$ were kept constant and the scattered intensity has been measured as a function of the in-plane angle 2θ. The angles $\alpha_{i,s}$ were chosen so that the scan trajectory in reciprocal space passed the coherent truncation rod in a very small distance $Q_x = 2.5 \times 10^{-3}$ nm^{-1}, in order to exclude the specular intensity peak from the measurements. For various values of $\alpha_{i,s}$ (i.e., for different Q_z values), pairs of GISAXS scans were recorded for two azimuthal positions of the sample, namely, with $Q_y \| [100]$, Fig. 2(a), and with $Q_y \| [010]$, Fig. 2(b).

The results of the GISAXS measurements are plotted in Fig. 3 for various Q_z. For the first scan the information depth[15] is much smaller than the multilayer period D, and for the second scan it corresponds to about $D/2$, whereas for all other scans it is much larger than this period. Thus, except the first two, the scans give information mainly on the *average* structure of the wires in the multilayer. In arrangement (a), the GISAXS data show a periodic sequence of satellite intensity maxima, while in (b) only a central peak can be seen. Thus, similarly to the ripples observed at the surface, the buried wires are nearly periodically arranged along [100], i.e., along the miscut, and no periodic structure is present in the [010] direction.
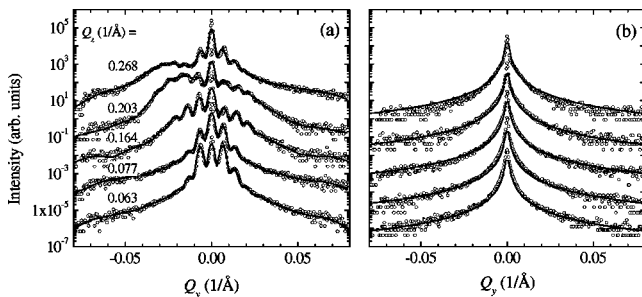
FIG. 3. GISAXS scans (circles) measured for different Q_z in the two arrangements of Fig. 2. Lines represent simulations. Curves are shifted vertically for clarity.

III. THEORY

From the comparison of the measured scans with simulated ones, we can determine an average shape and the arrangement of the buried wires. The simulation is based on the distorted-wave Born approximation,[16] with a semi-infinite Si substrate as undisturbed system. In the following, we denote $\Omega(\mathbf{r})$ the shape function of an individual buried wire; this function equals unity inside the wire and zero outside it. We express it in the coordinate system $x_{1,2,3}$, where x_3 is parallel to the vertical [001] z axis, x_2 is directed along the wires (direction [010]) and x_1 across them, i.e., along $[\bar{1}00]$ (see Fig. 2). In the arrangements (a) and (b), the x_1 axis is parallel to the y and x axes, respectively.

The x-ray scattering is calculated by means of the distorted-wave Born approximation.[15,16] Within this approach, the primary wave is transmitted through the sample surface, then scattered by the buried wires, and the scattered wave is transmitted through the sample surface as well. Assuming that all the buried wires have the same shape, the reciprocal space distribution of the intensity scattered diffusely from the buried wires is[15]

$$I(\mathbf{Q}) = \text{const.}|t_i t_s|^2 |\Omega^{\text{FT}}(\mathbf{Q}_T)|^2 C(\mathbf{Q}_T), \qquad (1)$$

where $\mathbf{Q} = (Q_x, Q_y, Q_z)$ and $\mathbf{Q}_T = (Q_x, Q_y, Q_{Tz})$ are the scattering vectors in vacuum and corrected to refraction and absorption in the undisturbed structure, respectively. $t_{i,s}$ are the Fresnel transmittivities of the surface of the undisturbed system, and FT denotes the Fourier transformation.

$$C(\mathbf{Q}_T) = \left\langle \sum_{m,n} \exp[-i(\mathbf{R}_m \cdot \mathbf{Q}_T - \mathbf{R}_n \cdot \mathbf{Q}_T^*)] \right\rangle$$

is the correlation function of the wire positions, where the vector $\mathbf{R}_m = (X_{1m}, 0, X_{3m})$ denotes the position of the mth wire. The correlation function is a product of the lateral and vertical correlation functions $C = C_\| C_\perp$. The vertical correlation function $C_\perp(\mathbf{Q}_T)$ describes the correlation of the wire positions at different interfaces. Due to their strain fields, wires at different interfaces are arranged along lines inclined by an angle χ (replication angle) from the growth direction.[17–19] This oblique arrangement of wires is manifested by the concentration of the scattered intensity $I(\mathbf{Q})$ into sheets in reciprocal space, as is indicated in Fig. 4. The vertical distance of the sheets is $2\pi/D$ and they are inclined by χ from the horizontal direction.[18,19] Two-dimensional intensity distributions of our sample measured in coplanar diffraction and coplanar small-angle scattering, exhibit nearly horizontal intensity sheets $[\chi = (3 \pm 3)°]$, i.e., the wires at different interfaces are arranged vertically. Then, the vertical correlation function $C_\perp(\mathbf{Q}_T)$ depends only on Q_{3T}, which is constant in a GISAXS scan, and $C_\perp(\mathbf{Q}_T)$ can be included in the constant factor in Eq. (1).

The form of the lateral correlation function can be chosen assuming that the lateral wire positions obey the short-range-order (SRO) model, i.e., the lateral distances of the wires l are random with the mean value $\langle l \rangle = L$, and the neighboring distances are not correlated.[20] Within the SRO model, the lateral correlation function is obtained as the statistical aver-
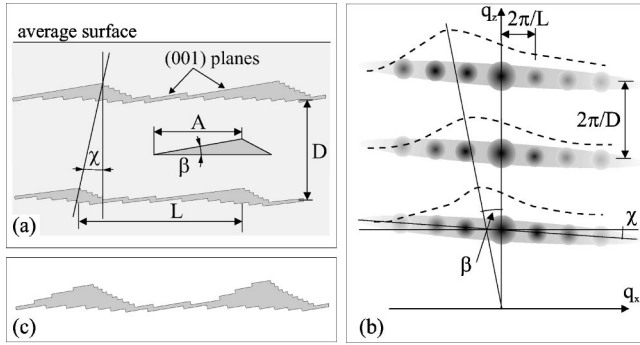
FIG. 4. (a) Sketch of the wire arrangement, (b) corresponding intensity distribution in reciprocal space. (c) Sketch of the distribution of steps forming the wires.

FIG. 5. Coefficients F_p determined from the GISAXS scans measured in the arrangement (a) (points) and their simulations (lines). Arrows indicate the positions of the side maxima of the envelope curves (shifted vertically for clarity).

age of geometrical factors of many perfectly periodic wire sequences with various random distances l. Since the geometrical factor of a perfectly periodic wire sequence is proportional to a periodic sequence of δ-like peaks centered in the corresponding reciprocal lattice points, the resulting lateral correlation function is

$$C_\parallel(Q_1) = M \left\langle g \sum_{p=-\infty}^{\infty} \delta(Q_1 - pg) \right\rangle, \quad g = 2\pi/l, \quad (2)$$

where M is the number of the wires at the same interface and the averaging is performed over the random distances l. Putting this form of the correlation function into Eq. (1) we obtain the final formula for the scattered intensity

$$I(\mathbf{Q}) \sim |t_i t_s|^2 \left[\delta(Q_1) F_0 + \sum_{p \neq 0} \frac{F_p}{|p|} w\left(\left| \frac{Q_1}{p} \right| \right) \right], \quad (3)$$

where $F_p(Q_2, Q_{3T}) = |\Omega^{FT}(Q_1 = pG, Q_2, Q_{3T})|^2$ are the values of $|\Omega^{FT}(\mathbf{Q}_T)|^2$ in the lateral satellites, and $w(g)$ is the probability distribution function of the random quantity g. Equation (3) describes a sequence of lateral satellite maxima along Q_1, with period $G = 2\pi/L$. The width of the satellites increases with the satellite order and the intensity exhibits a δ-like peak at $Q_1 = 0$. In the measured data, this peak is broadened by goniometer resolution and/or by the coherence properties of the primary x-ray beam.

IV. RESULTS AND DISCUSSION

In arrangement (b), $Q_1 \equiv Q_x = \text{const} \approx 0$, $Q_2 \equiv Q_y$, $Q_3 \equiv Q_z$, and the scan trajectory is perpendicular to the sequence of intensity satellites. Then, only a central peak can be found in the measured data. If we assume that the actual wire lengths b along x_2 are randomly distributed with the exponential probability distribution with mean value B, the shape of the maximum is Lorentzian. Fitting the measured scans with Lorentzian curves [see Fig. 3(b)], we obtain $B = (250 \pm 50)$ nm, in good agreement with the AFM data of the sample surface.

In arrangement (a), $Q_1 \equiv -Q_y$, $Q_2 \equiv Q_x = \text{const} \approx 0$, $Q_3 \equiv Q_z$, and the trajectory of the GISAXS scan is perpendicular to the wires and crosses the lateral satellites. We have fitted these scans using Eq. (3), the fitted curves are plotted
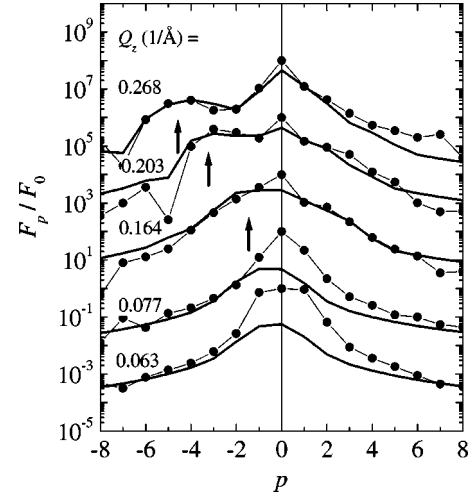
in Fig. 3. The resulting parameters are the mean wire distance $L = (90 \pm 5)$ nm, its root-mean-square deviation $\sigma_L = (15 \pm 5)$ nm, and the coefficients $F_p(0, Q_{Tz})$. The measured and calculated curves coincide perfectly, indicating that the wire positions are very well described by the SRO model.

The coefficients F_p, which are plotted in Fig. 5, contain information on the wire shape, which influences the envelope of the lateral maxima. However, a direct reconstruction of the shape function $\Omega(\mathbf{r})$ from the F_p is not possible, since the phase information of Ω^{FT} is missing. Therefore, we assume a suitable model of the wire structure and determine its parameters from the comparison with the experimental values of F_p. From Fig. 5 it follows that, apart from the central peak at $p = 0$, the envelope curve of the satellite maxima exhibits a side maximum for larger Q_{Tz}. This maximum shifts to negative p's, and the shift is proportional to Q_{Tz}. This behavior indicates that the wire cross section has a distinct ''facet'' making an angle β with the average interface. We use the quoted term ''facet,'' because it seems unlikely that what we observe is really a crystallographic facet; since we are investigating *buried* structures, one might think of a facet that is disturbed and rounded during overgrowth.

Qualitatively, such a ''facet'' could be explained for wires formed by step bunching, as is illustrated in Fig. 4(a); SiGe-rich wires form at step bunches, where the accumulation of steps allows for a better elastic relaxation of SiGe. If no steps occur at one side of the wire, a (001) facet is formed, which is inclined exactly by the miscut angle (in our case $3.5 \pm 0.02°$) with respect to the average interface. This leads to a triangular shape of the wires, with one side inclined by an angle β and a horizontal base [see inset in Fig. 4(a)]. Due to the tendency of flattening of self-organized structures during overgrowth, one would expect β to be somewhat *smaller* than the miscut angle.[4,18,19] The amplitude of the ripples at the Si to SiGe interface should be similar to that observed for the surface ripples by AFM, which are

about 0.4 nm high, much less than the wire height (see below), hence the lower interface of the wires can be assumed to be flat. For the simulations, we used β, the facet width A [see Fig. 4(a)] and its fluctuation σ_A as free parameters. Because β is small, A corresponds also to the width of the wire, the right-hand side of the wire is much steeper, and the corresponding streak in the GISAXS scans cannot be observed, as it influences the envelope of the satellite peaks only at very large values of Q_y.

In reciprocal space, the side maxima of the *envelope* curves for various Q_{Tz} lie at a line perpendicular to the facet. This is shown in Fig. 4(b), where we depicted how the features in reciprocal space correspond to the real-space features of the wires.

From the shift Δp of the maximum for a given ΔQ_{Tz} we get $\beta = \arctan(G\Delta p/\Delta Q_{Tz})$. The width A of the wire is inversely proportional to the width of this maximum. The central maximum of the envelope curve stems from the base of the wires and the wetting layers between the wires, but is also influenced by, e.g., diffuse scattering from usual interface roughness between the wires. The calculated envelope curves are plotted in Fig. 5. We found $\beta = (6\pm1)°$, $A = (35\pm5)$ nm, and $\sigma_A = (10\pm5)$ nm, and a resulting height of the wires of about 3.7 ± 1.2 nm. The shape of the experimental envelope curve is well reproduced by the model, the experimental central peak is somewhat higher due to the scattering from the areas between the wires. The discrepancy between the simulation results and the F_p values for the smallest Q_z are probably caused by the scattering from the holes at the surface observed by AFM (Fig. 1), and by the surface ripples, as their shape (height) differs from that of the buried wires.

Although the triangular model is a simplifying assumption on the wire shape, the presence of a facet inclined by about $6°$ with respect to the average interfaces is obvious. Remarkably and unexpectedly, this angle is *larger* than the crystallographic miscut ($3.5°$), hence the facet is more inclined to the mean interface than the crystallographic (001) plane. The measured β would correspond to a very highly indexed plane as $(1\,0\,18)$, hence what we observe is not likely a crystallographic facet. However, there is an important consequence for the understanding of the growth pro-

cess: With respect to the (001) plane, the measured angle means that the wires are formed not solely by a bunching of ''downward'' steps, as sketched in Fig. 4(a), but contain also ''upward'' steps [Fig. 4(c)]. It cannot be decided from our experiment, and might challenge the further improvement of growth models, whether this indicates that already during the deposition of SiGe, upward steps are formed, e.g., due to kinetic limitations of the growth process,[21] or if the slope steeper than the miscut is formed during overgrowth of the SiGe wires with Si. However, as generally a trend of *flattening* of self-organized structures during overgrowth is observed,[12,13] it seems much more probable that the upward steps are formed already during deposition of SiGe.

V. SUMMARY

In conclusion, self-organized buried SiGe wires in a Si/SiGe multilayer sample, grown on a vicinal Si substrate with a rather large miscut angle, were investigated by grazing incidence small-angle x-ray scattering. The scattering data prove that laterally periodically arranged buried SiGe wires are present, which are elongated parallel to the monolayer steps of the vicinal surface. The scattered intensity was analyzed using a model based on the distorted wave Born approximation. We have found that the lateral wire distribution obeys the short-range-order model, the mean distance of the buried wires equals that of the ripples at the sample surface. From the heights of the lateral satellite maxima we determined the mean width of the wire to be 35 nm (i.e., less than the half of the wire distance) and the angle of its side facet to $6°$. Since this angle is larger than the crystallographic miscut, the self-organization process creating the wires cannot be explained by the bunching of monolayer steps alone.

*Permanent address: Department of Solid State Physics, Faculty of Science, Masaryk University, 611 37 Brno, Czech Republic.

†Email address: g.bauer@hlphys.uni-linz.ac.at

[1] M. Schmidbauer, Th. Wiebach, H. Raidt, M. Hanke, R. Koehler, and H. Wawra, Phys. Rev. B **58**, 10 523 (1998).

[2] M. Rauscher, R. Paniago, T.H. Metzger, Z. Kovats, J. Domke, J. Peisl, H.D. Pfannes, J. Schulze, and I. Eisele, J. Appl. Phys. **86**, 6763 (1999).

[3] J. Stangl, V. Holý, A. Daniel, T. Roch, G. Bauer, J. Zhu, K. Brunner, and G. Abstreiter, Phys. Rev. B **62**, 7229 (2000).

[4] V. Holý, C. Giannini, L. Tapfer, T. Marschner, and W. Stolz, Phys. Rev. B **55**, 9960 (1997).

[5] A.A. Darhuber, J. Zhu, V. Holý, J. Stangl, P. Mikulík, K. Brunner, G. Abstreiter, and G. Bauer, Appl. Phys. Lett. **73**, 1535 (1998).

[6] C. Giannini, T. Baumbach, D. Luebbert, R. Felici, L. Tapfer, T. Marschner, W. Stolz, N.Y. Jin-Philipp, and F. Philipp, Phys. Rev. B **61**, 2173 (2000).

[7] H. Omi and T. Ogino, Appl. Phys. Lett. **71**, 2163 (1997).

[8] J. Zhu, K. Brunner, and G. Abstreiter, Appl. Phys. Lett. **73**, 620 (1998).

[9] F. Liu, J. Tersoff, and M.G. Lagally, Phys. Rev. Lett. **80**, 1268 (1998).

[10] K. Brunner, J. Zhu, C. Miesner, G. Abstreiter, O. Kienzle, and F. Ernst, Physica E (Amsterdam) **7**, 881 (2000).

[11] T. Baumbach, D. Lübbert, and M. Gailhanou, J. Appl. Phys. **87**, 3744 (2000).

[12] O.G. Schmidt, U. Denker, K. Eberl, O. Kienzle, and F. Ernst, Appl. Phys. Lett. **77**, 2509 (2000).

[13] P. Sutter and M.G. Lagally, Phys. Rev. Lett. **81**, 3471 (1998).

[14] C. Schelling, G. Springholz, and F. Schäffler, Phys. Rev. Lett. **83**, 995 (1999).

[15] V. Holý, U. Pietsch, and T. Baumbach, *High Resolution X-Ray Scattering from Thin Layers and Multilayers*, Springer Tracts in Moder Physics Vol. 149 (Springer-Verlag, Berlin, 1999).

[16] S.K. Sinha, E.B. Sirota, S. Garoff, and H.B. Stanley, Phys. Rev. B **38**, 2297 (1988).

[17] J. Tersoff, Y.H. Phang, Z. Zhang, and M.G. Lagally, Phys. Rev. Lett. **75**, 2730 (1995).

[18] V. Holý, A.A. Darhuber, J. Stangl, G. Bauer, J. Nützel, and G. Abstreiter, Semicond. Sci. Technol. **13**, 590 (1998).

[19] V. Holý, A.A. Darhuber, J. Stangl, G. Bauer, J. Nützel, and G. Abstreiter, Phys. Rev. B **57**, 12 435 (1998).

[20] P.R. Pukite, C.S. Lent, and P.I. Cohen, Surf. Sci. **161**, 39 (1985).

[21] C. Schelling, G. Springholz, and F. Schäffler, Thin Solid Films **369**, 1 (2000).